Advanced Powder Technology 24 (2013) 1063–1069

Contents lists available at SciVerse ScienceDirect

Advanced Powder Technology

journal homepage: www.elsevier.com/locate/apt

Original Research Paper

Evolution of the phase stability of Ni–Al under low energy ball milling

E. Zelaya [a,*], M.R. Esquivel [a,b], D. Schryvers [c]

[a] Centro Atómico Bariloche – CNEA, Av. Bustillo 9500. CONICET, 8400 S.C. de Bariloche, Argentina
[b] UNCo, Quintral 1250, 8400 S.C. de Bariloche, Argentina
[c] EMAT, University of Antwerp, Groenenborgerlaan 171, Antwerp, Belgium

ARTICLE INFO

Article history:
Received 20 August 2012
Received in revised form 28 February 2013
Accepted 15 March 2013
Available online 30 March 2013

Keywords:
Intermetallics
Mechanical alloying
Microstructure
Transmission electron microscopy
X-ray diffraction

ABSTRACT

Low energy mechanical alloying of Ni–35 at.%Al and Ni–40 at.%Al material was performed and the resulting structures were investigated by XRD and TEM. The final intermetallics observed consist of two phases, NiAl(B2) and Ni_3Al while 7R and 3R martensite was observed in post-annealed samples. Different integrated milling times were associated to the intermetallic consolidation and initial blend dissociation.

1. Introduction

Ni–Al alloys are attractive due to a good performance at high temperatures and in aggressive environments. As a result, this alloy has potential applications in hot sections of gas turbine engines for aircraft–propulsion systems, bond coats under thermal barrier coatings, electronic metallization compounds in advanced semiconductor heterostructures, surface catalysts, etc. [1]. Ni–Al also possesses a high melting point and a high oxidation resistance at high temperatures ($T > 1100$ °C). However, the synthesis of alloys with constituents having a large difference in melting temperatures, in this case around 800 °C difference between Ni and Al, increases the costs of conventional thermal fabrication methods [2,3]. Therefore, it is commercially attractive to develop synthesis processes of Ni–Al alloys based on a solid–solid reaction produced by mechanical alloying (MA). Low energy mechanical alloying is performed at low temperatures ($T < 150$ °C) and this technique is an effective method to produce equilibrium as well as non-equilibrium phases [4,5]. Low energy milling also allows a detailed study of the processing since the integrated milling time needed to reach the final composition is longer than those of intermediate or high energy mechanical alloying allowing for easier identification of processing stages at intermediate synthesis.

At 400 °C and 35 at.%Al, the Ni–Al equilibrium phase diagram indicates the existence of the orthorhombic Ni_5Al_3 structure [6]. For higher Ni concentration, the cubic Ni_3Al structure is stable in a narrow region of 2 at.%. Around 40 at.%Al the phase diagram indicates the coexistence of the Ni_5Al_3 structure with the cubic B2 (CsCl-type, ordered bcc). This B2 phase appears as a stable phase in a range of nearly 13 at.% width and undergoes a reversible martensitic transformation at low temperatures, provided it is rapidly quenched to suppress possible phase decomposition [7,8]. The martensite has the $L1_0$ structure (CuAu ordered fct) with either ABC (3R) stacking or ABCABAC (7R/7M/14M) stacking, depending on the alloy composition and stress conditions. The martensitic transformation temperature varies linearly and decreases strongly as the Al content of the sample increases. The martensite structure also varies from 7R to 3R with increasing Ni content, with approximately 63 at.%Ni as a critical composition [9–12].

The 3R, B2 and Ni_5Al_3 structures can coexist in the same bulk sample at 35 at.%Al by changing the heat treatment [13–16]. Moreover, in a similar sample a microstructure transition from 3R to 7R was found [17]. It was attributed to a Ni-depletion effect in the matrix caused by Ni-enrichment in the globular Ni_5Al_3 precipitation zones. While various phases could be found coexisting in Ni–Al samples with the same composition of those in the present work, intermediate and high energy ball milling seems to produce fewer phases for this composition [18,19]. Ni_3Al + NiAl were reported as final intermetallic after 30 h in a planetary mill [18], Ni(Al) was found after 5 h in a vibratory ball mill under argon atmosphere at room temperature and Ni_3Al was obtained after heating of MA to 700 °C in a calorimeter [19] (Table 1). At 40 at.%Al only NiAl(B2) was found as the final intermetallic produced in a planetary mill after 30 h [18], while Ni_3Al + NiAl were reported as final intermetallic found after 5 h in a vibratory ball mill and heat treated to

* Corresponding author.
E-mail addresses: zelaya@cab.cnea.gov.ar, euge.zelaya@gmail.com (E. Zelaya).

0921-8831/$ - see front matter
http://dx.doi.org/10.1016/j.apt.2013.03.008

Table 1
Milling times and general characteristics of XRD and TEM analysis for 35Al. The main difference between both techniques is noticed in samples 35/20 and 35/50. For comparison, the data obtained in earlier work at high and intermediate energy milling is also shown.

Sample	Type mill	Integrated milling time (h)	XRD	TEM		Ref.
				ring diff. pattern + EDS + HRTEM	Average grain size (nm)	
35/3	Low energy	3	Ni + Al	Ni + Al		This work
–	High energy	5 + heat to 700 °C	Ni_3Al	–	–	[19]
35/10	Low energy	10	Ni + Al	Ni + Al		This work
35/20	Low energy	20	Ni + Al	NiAl ± Ni_3Al	17 ± 14	This work
–	Interm. energy	30	NiAl + Ni_3Al	–	10	[18]
35/50	Low energy	50	NiAl + Ni_3Al	NiAl + Ni_3Al + Ni	6 ± 6	This work
35/100	Low energy	100	NiAl + Ni_3Al	NiAl + Ni_3Al	3 ± 3	This work
35/100/24	Low energy	100 h + 24 h at 600 °C	NiAl + Ni_3Al + 7R	NiAl + Ni_3Al + 7R + 3R	50 ± 30	This work

Table 2
Milling times and general characteristics of XRD and TEM analysis for 40Al. The main difference between both techniques is noticed in sample 40/100. For comparison, the data obtained in earlier work at high and intermediate energy milling is also shown.

Sample	Type mill	Integrated milling time (h)	XRD	TEM ring diff. pattern + EDS + HRTEM analysis	Average grain size (nm)	Ref.
40/3	Low energy	3	Ni + Al	–	–	This work
–	High energy	5 + heat to 700 °C	Ni_3Al + NiAl			[19]
40/10	Low energy	10	Ni + Al Cold welding	–	–	This work
40/20	Low energy	20	Ni + Al + NiAl	Ni + Al + NiAl	(9 ± 13) and (108 ± 13)	This work
–	Interm. energy	30			10	[18]
40/50	Low energy	50	Ni + NiAl	Ni + NiAl	(8 ± 5) and (58 ± 12)	This work
40/100	Low energy	100	NiAl	Ni + NiAl	(7 ± 4) and (32 ± 4)	This work

700 °C in a calorimeter [19] (Table 2). It should also be noted that neither of the intermediate or high energy milling processes produce the equilibrium intermetallic according to the phase diagram [2] for any of the used compositions.

The present work identifies and characterizes the phases present after a combination of low energy mechanical alloying and heat treatments and compares the evolution of the intermetallics found by various techniques using two different start compositions. While X-ray preserves the statistical viewpoint of the intermetallic results, TEM provides a detailed observation of the initiation of each process in the reactive alloying [20].

2. Materials and methods

Nickel powder (99.999% purity, 5 μm) and aluminum flakes (99.999% purity, 5 mm) were combined in ratios of Ni–35 at.%Al (35Al) and Ni–40 at.%Al (40Al). From the profiles of XRD patterns the size of the grains in the original constituents was estimated as 70 nm for Al and 150 nm for Ni. The milling was carried out in a horizontal-motioned mill (Uniball Mill II-Australian Instruments). Milling processing and sample handling was done under Ar atmosphere (99.999%) at controlled conditions (humidity < 100 ppm, O_2 content < 5 ppm). A mass ratio of steel balls to the elemental blends of 22.33:1 was selected in order to favor a low energy ball milling at 140 rpm. After certain intervals of time, powder samples of 200 mg were taken for X-ray and TEM analysis. In what follows, samples are labeled with their Al concentration and milling time, e.g., 35/20 stands for 35Al milled for 20 h (Tables 1 and 2). Room temperature X-ray diffraction was performed on a Philips PW 1710/01 Instrument with Cu Kα radiation. X-ray diffraction patterns were analyzed by the Rietveld method using DBWS software [21]. SEM images were acquired in an FEI 515 with an EDAX 9900 spectrometer for EDS analysis. TEM characterization was performed using an FEI Tecnai F20 G2 field emission microscope and an FEI CM200 UT, both operating at 200 keV.

The thermal stability of the MA products was examined using a TA 2910 DSC. The sample was measured from room temperature to 500 °C in a purified Ar (99.999%) atmosphere at a rate of 5 °C min^{-1}.

3. Results

The evolution of the phases for both compositions (35Al and 40Al) can be observed in Fig. 1. The average mass percentages are estimated from the Rietveld analysis, the lines are a guide for the eye. Neither X-ray peak identification nor TEM EDS reveals any contamination of previous milling or vial elements in the particles analyzed.

Fig. 2a–c show dark field images of particles with an initial composition of 35Al for three different integrated milling times. As the milling time increases, as shown here from 20 to 100 h, a decrease of the grain size, even inside particles of similar size, is observed (values are given in Tables 1 and 2). Also the average particle size increases with milling time. Simultaneously, a broadening of the

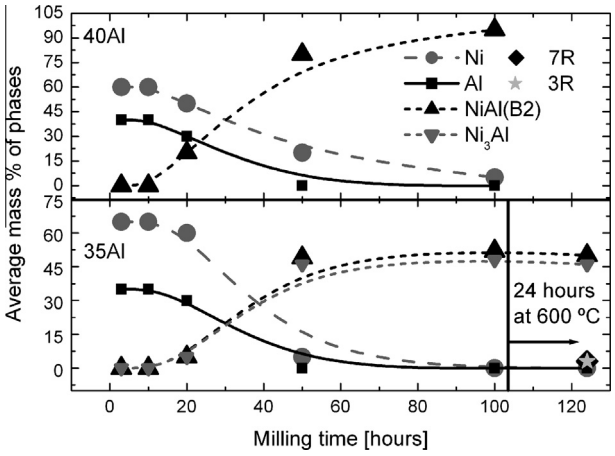

Fig. 1. Evolution of the phases as the milling time increases for samples 40Al (up) and 35Al (down). The mass percentages are estimated from the Rietveld analyses.

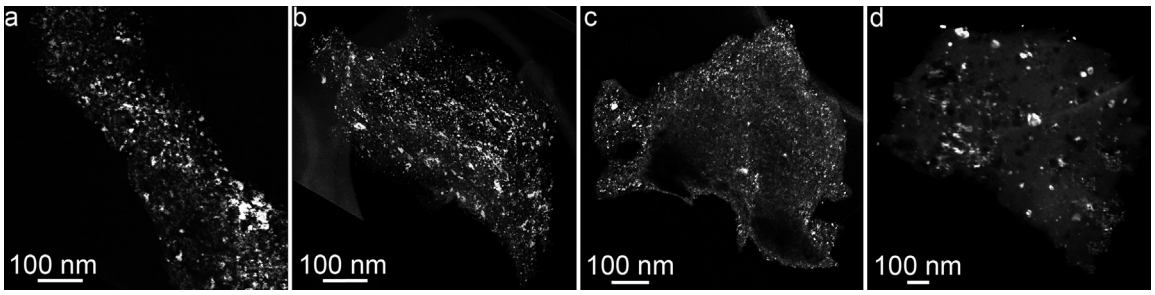

Fig. 2. Dark field images of samples 35Al (a) milled for 20 h, (b) milled for 50 h, (c) milled for 100 h and (d) milled for 100 h and heated for 24 h at 600 °C. As the milling time increases, the average grain size decreases. The sample heated for 24 h shows grain sizes twice as large as the as-milled counterpart.

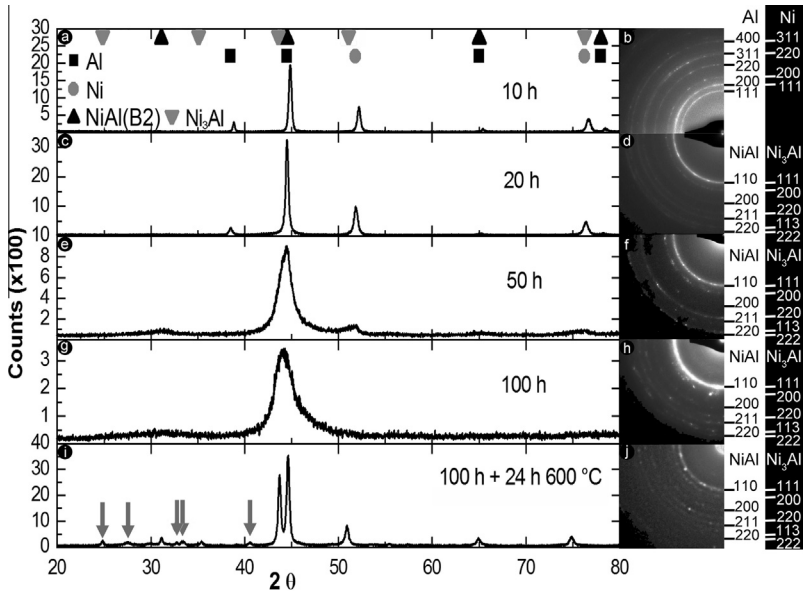

Fig. 3. X-ray diffraction patterns of the as-milled 35Al samples (a) 10 h, (c) 20 h, (e) 50 h, (g) 100 h and (i) milled for 100 h and annealed at 600 °C for 24 h. Single quadrant TEM ring diffraction patterns of as-milled samples (b) 10 h, (d) 20 h, (f) 50 h, (h) 100 h and (j) milled for 100 h and heated for 24 h at 600 °C. The broadening of intensity for each ring as the milling time increases is clear. The annealed sample shows peak splitting of the mean ring and the appearance of several small peaks in the XRD. The grey arrows in (i) point at peaks of the 7R phase.

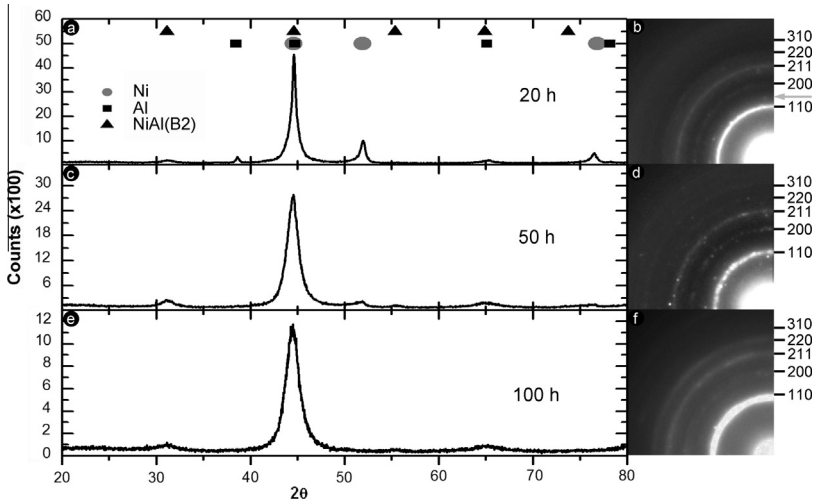

Fig. 4. X-ray diffraction patterns of the as-milled 40Al samples (a) 20 h, (c) 50 h, and (e) 100 h. Single quadrant TEM ring diffraction patterns of the as-milled samples (b) 20 h, (d) 50 h, and (f) 100 h.

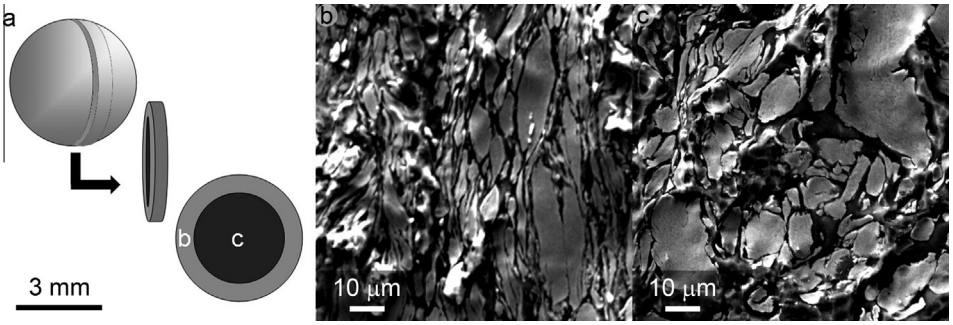

Fig. 5. (a) Scheme of the cut performed on a single core–shell particle of sample 40/10. (b) and (c) SEM backscatter micrographs of the respective areas indicated in (a), revealing a clear difference in morphology between core and shell.

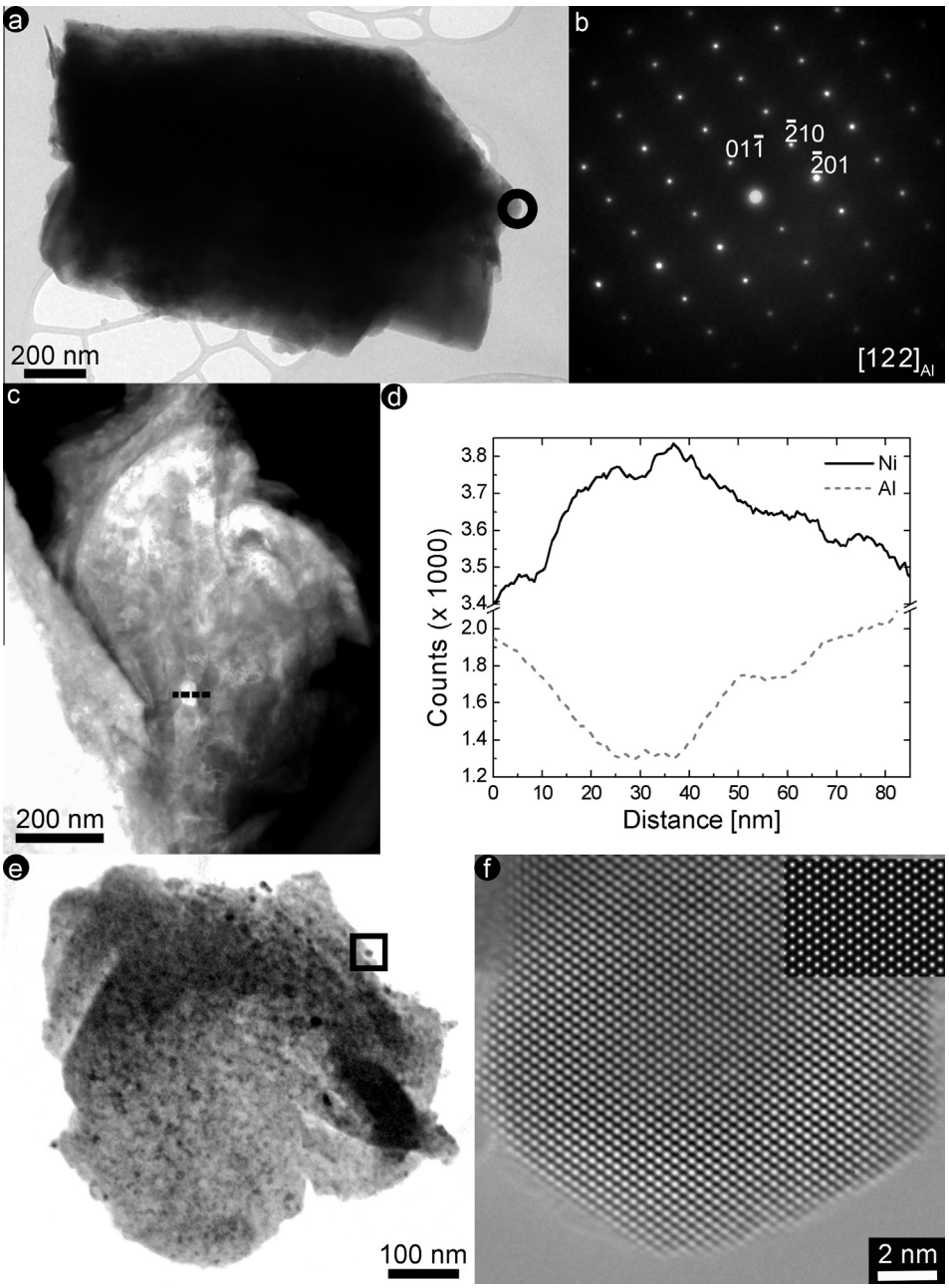

Fig. 6. (a) Bright field image of the sample 40/20. (b) Microdiffraction pattern of the area circled in (a) and indexed as $[1\,2\,2]_{Al}$ zone axis. (c) HAADF-STEM image of sample 35/50. The dashed line indicates the region of the compositional analysis. (d) EDX line-scan across a Ni-rich region inside a Ni–Al particle with ring patterns consistent with a Ni–Al intermetallic. (e) Bright field image of the sample 40/100. (f) HRTEM image of the square area in (e) and inset of matching a [1 1 0] HRTEM simulation of Ni for a defocus value of 58 nm and a thickness of 5.5 nm.

peaks in TEM ring diffraction patterns and X-ray diffractograms is observed as presented in Figs. 3 and 4 for both compositions.

3.1. After 3 h of milling

X-ray diffractograms show no evidence of intermetallic formation for any of the selected compositions. The TEM ring diffraction also only shows the presence of the individual structures of Al and Ni for both initial compositions.

3.2. After 10 h of milling

Although the X-ray diffractograms of both compositions did not show any peaks related to the formation of any intermetallic, the morphologies of the ball-milled samples do present differences. Sample 35/10 is a powdered one while sample 40/10 shows solid spheres between (2.5 ± 0.1) mm and (4.0 ± 0.1) mm in diameter with a core–shell type of structure. The SEM backscattered micrographs of Fig. 5b and c reveal in both areas a darker matrix with brighter islands. EDS performed over 20 different areas shows a 99 at.%Al in the matrix and a 99 at.%Ni in the islands, confirming the brightness differences in the EBS images. Even when the composition of the different areas is the same in both regions (shown as areas *b* and *c* in Fig. 5a) a different morphology of the islands is appreciated from the SEM micrograph. The islands near the sphere surface seem to be larger and elongated in the direction parallel to the surface while they are less textured in the interior.

3.3. After 20 h of milling

Peaks associated with an intermetallic phase could not be detected in sample 35/20 by XRD. However, the indexing of the corresponding TEM ring diffraction pattern is consistent with the presence of Ni_3Al and NiAl(B2) (Fig. 3). This inconsistence between both techniques will be further explained in the discussion.

Meanwhile the peaks of the X-ray diffractogram of sample 40/20 are consistent with the presence of Ni, Al and NiAl(B2). On the other hand, the TEM ring diffraction pattern could be indexed as a NiAl(B2) structure but a weak ring that is observed between 110 and 200 could also be attributed to the 220 reflection of Ni (arrow in Fig. 4b). Moreover, TEM microdiffraction performed on sample 40/20 revealed some small areas (~50 nm) with a diffraction pattern that can be indexed as a $[1\,2\,2]_{Al}$ zone axis (Fig. 6a and b).

3.4. After 50 h of milling

Rietveld analysis of sample 35/50 indicates the presence of Ni_3Al and NiAl(B2) while no pure element peaks were detected anymore. This was confirmed by the TEM ring diffraction. However, the STEM image shown in Fig. 6c and a line scan performed over the same bright area shown in Fig. 6d revealed a Ni-rich area of 20 nm diameter.

The X-ray diffractogram of sample 40/50 shows peaks associated to Ni and NiAl(B2) while the TEM ring diffraction pattern can be indexed with a NiAl(B2) structure (Fig. 4c and d). However, HRTEM shows images that match with the simulation of [1 1 0] Ni (not shown).

3.5. After 100 h of milling

Using various TEM techniques Ni_3Al and NiAl(B2) were detected in sample 35/100 while only NiAl(B2) was detected in sample 40/100. No evidence of pure metals was detected in sample 35/100, but a HRTEM image of sample 40/100 could be attributed to Ni observed along the [0 1 1] zone axis (Fig. 6e and f).

Table 3
Structural parameters of the intermetallics found in sample 35Al.

Compound	Cell parameters		Atoms				
			At	Wy	*x*	*y*	*z*
Ni_3Al	*a*, *b*, *c* (nm)	0.3574(3)	Al	a	0.00	0.00	0.00
	α, β, γ	90°	Ni	c	0.50	0.50	0.00
NiAl (B2)	*a*, *b*, *c* (nm)	0.2861(7)	Al	a	0.00	0.00	0.00
	α, β, γ	90°	Ni	a	0.50	0.50	0.50

The Rietveld analyses of samples 35/100 and 40/100 are again consistent with the presence of intermetallics without pure elements. However, a HRTEM image of sample 35/100 shows an image that matches with the simulation of a Ni_3Al structure along the [1 1 0] zone axis but with a different lattice parameter than the one reported in Table 3: $a = (4.0 \pm 0.2)$ Å instead of $a = (3.6 \pm 0.2)$ Å (Fig. 7a and b).

3.6. Heat treatments after 100 h of milling

Figs. 2 and 3 show the effect of one heat treatment of 600 °C for 24 h of the 35Al sample. Similar heat treatments were performed for different temperatures (400 °C and 800 °C) and shorter annealing times showing similar characteristics but less pronounced.

The Rietveld analysis of the X-ray diffractogram of this sample agrees with the presence of two major phases Ni_3Al and NiAl(B2) and the minor 7R phase. Not all peaks observed by X-ray for this last phase are shown in Fig. 3 since the main peaks of NiAl(B2) and Ni_3Al are superimposed to the ones of 7R. For example, the reflections (1 0 6) and (2 0 1) of 7R are superimposed to those of NiAl(B2) (1 1 0) $2\theta = 43.71$ and Ni_3Al (1 1 1) $2\theta = 44.59$, the two major reflections observed in the diffractogram. Also a HRTEM micrograph of this sample shown in Fig. 7c and d reveals an image consistent with the (5–2) stacking of the 7R structure. In fact, in the top part of the zoom of Fig. 7d also a 3R stacking is observed, although no evidence for this structure was found in the XRD patterns.

The heat treatments on sample 40/100 show no modification in the detection of the phases using the Rietveld method.

4. Discussion

4.1. Morphology and microstructure

The dark field images of the particles in Fig. 2 show the decrease of the average grain size as the milling time increases. Also the broadening of the X-ray diffractograms and the TEM ring diffraction patterns indicate a reduction of the average grain size (Figs. 3 and 4). During mechanical alloying of Ni and Al, the powders and flakes agglomerate reaching the initial and intermediate milling stages [5]. Since these stages are dominated by fracture, the formation of a system with smaller average grain size is indeed favored. This process involves a solid–solid diffusion and is energetically favorable for the nucleation of intermetallic phases. The same behavior in the decrease of the grain size could be seen using a high energy ball mill in the same intermetallic system [22].

The sample with the highest amount of Al and milled for 10 h showed the characteristic morphology of the dominant effects of cold welding in a ductile (Al)–brittle (Ni) mixture with greater abundance of the ductile constituent leading to the formation of core–shell spheres as shown in the schematic of Fig. 5a. This is a typical example of a process that occurs at intermediate milling times and that can only be observed in low energy milling since this technique allows a more detailed study of intermediate stages than possible in a high energy experiment. By analyzing the composition of the interior of the sample it was found that the initial

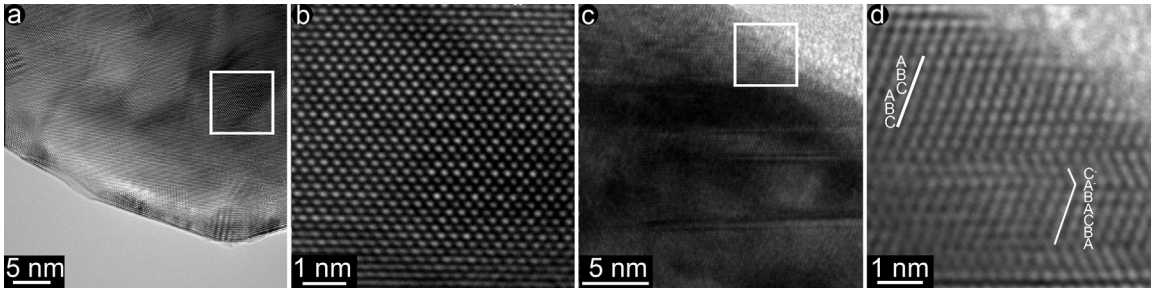

Fig. 7. (a) HRTEM image of sample 35/100. (b) Zoom of the area inside the white line square in (a) showing a symmetry consistent with a [1 1 0] zone axis of Ni_3Al. (c) HRTEM image of sample 35/100/24. (d) Zoom of the area inside the white line square in (c) showing the (5–2) stacking of the 7R structure and the 3R stacking sequence (Table 3).

metals maintained their own identity, forming a compound of islands of Ni in a continuous matrix of Al as shown in Fig. 5b and c. The morphology of the islands observed in the outer zone of the spheres is elongated parallel to the outer surface of the sphere. This morphology is similar to the one obtained in a lamination process but does not appear in the interior of the spheres. This tendency in the peripheral part of the sphere yields thinner Ni islands which favor more solid–solid diffusion which is the dominant alloying mechanism at the present stage and under the milling energy applied. In turn, it favors the consequent formation of the intermetallics. In the present case Al flakes are larger (average size 5 mm) than Ni powder particles (mesh 100) and since Al is more ductile than Ni, the repetitive welding and fracturing of the powders will occur in the Al matrix. The identification of such dominant morphologies is another example of the detailed mechanism of formation of the intemetallics that can only be observed in low energy mills.

Fig. 1 shows that for both compositions the expected intermetallics are effectively formed under the used low energy milling conditions. However, based on the X-ray evidence it can be concluded that longer milling times are required to obtain the final stage for sample 35Al than for sample 40Al. For the 35Al sample, the final intermetallic phases consist of both NiAl(B2) and Ni_3Al, whereas for the 40Al sample only the NiAl(B2) structure is recognized.

4.2. Intermetallic phases

The different constituents and intermetallic phases were identified using X-ray diffraction, TEM selected area diffraction and HR(S)TEM imaging aided by EDS. With the used instrumentation powder X-ray diffractogram peaks can be observed and identified when crystallite sizes are larger than 20 nm. For smaller particles or grains the peaks are too wide to allow proper identification of phases [23]. Due to the width of the beam, such patterns, however, do provide a good overview of the appearing phases in sufficiently large grains. Using various TEM techniques, one can identify crystal structures in grain sizes as small as ~3 nm [24] which explains why some phases have been identified by TEM at lower milling times than possible with X-rays (e.g., NiAl + Ni_3Al in sample 35/20). On the other hand, due to the selectivity of the observed particles, TEM can sometimes overlook phases that occur with only a low frequency (e.g., Ni and Al in sample 35/20). A complete identification of (inter)metallic phases thus ideally uses a combination of these techniques.

The time required to detect a higher percentage of intermetallics was shorter for the sample that contains more Al (Figs. 1, 3 and 4). This might be surprising because a larger amount of Al should be milled for a longer time in order to reach a grain size similar to Ni and to form the intermetallic under the same milling conditions. However, the occurrence of core–shell spheres with thin Ni particles in the shell can explain the earlier formation of NiAl(B2) in the 40Al over NiAl(B2) + Ni_3Al in the 35Al sample.

The presence of intermetallics NiAl(B2) and Ni_3Al was first detected after 20 h of milling for both compositions. However, in the sample poorer in Al these phases could only be detected by TEM techniques. The samples richer in Al show a more heterogeneous grain size distribution with grains between 5 and 30 nm in diameter allowing the NiAl(B2) to be detected by X-ray diffractometry.

As the milling time increases, both X-ray and TEM diffractograms detect the intermetallic phases. However, in both concentrations Ni was occasionally detected, mostly using TEM.

The intermetallics detected in this work are not the equilibrium ones according to the phase diagram. However, the same intermetallics were detected for the same initial blends in a planetary ball-milling process [18]. On the contrary, the intermetallics obtained in a vibratory ball-mill followed by a heat treatment were NiAl(B2) + Ni_3Al for an initial composition near 40Al and NiAl(B2) for an initial composition near 35Al [19]. The balance of mass suggests that the last method involves a higher Ni loss by oxidation or preferential deposition in the chamber while the planetary ball-mill and the low energy ball-mill used in this work both lead to a loss of Al.

In the present work, a longer milling time was needed to produce a final intermetallic for both initial composition products when compared with intermediate or high energy milling. This can be explained by the fact that samples milled in low energy mills do not reach temperatures above 150 °C, which is correlated to slower and more local diffusion processes. This local solid–solid diffusion apparently also favors the local formation of more than one intermetallic.

The Ni_3Al phase detected in samples 35/20, 35/50, 35/100 and 35/100/24 was also reported in [19] and the diffractogram is close to the one presented in a melt-spun sample of 35Al [17]. In the latter work also Ni_3Al [9,10], NiAl(B2) and a 7R structure [25] were observed. However, the authors present some dissimilarities in the measured lattice parameters, which could be attributed to a local composition difference as mentioned in [17] or to the procedure used to obtain the material by melt spun or mechanical alloying.

In sample 35/100 the X-ray diffractogram (Fig. 3g) does not present a clear structure in the 20–40 2θ range, which can be related to the small crystallite size structure. TEM also confirms that the grain size is smaller than 6 nm while the powder particles are thicker and reveal less electron transparent areas. As a result the identification of any minority phase different from NiAl(B2) and Ni_3Al was difficult for both techniques in samples milled for 100 h. An annealing at 600 °C for 24 h followed by air quench was done in order to increase the crystallite size to reach a value easily analyzable for X-ray diffraction, although the possibility of creating new phases should not be overlooked. After this treatment, two structures with a larger lattice parameter could be

identified in the diffractogram (arrows in Fig. 3i), in addition to the intermetallics found in samples milled for more than 20 h. Even when the amount of this new structure is small the low angle of most of the peaks revealed after the heat treatment facilitates the identification of the structure. This structure reveals a seven layer stacking sequence that can also be distinguished in the HRTEM micrograph of Fig. 7d. The same (5,2) stacking sequence occurs in the low temperature martensite phase in Ni–Al samples with a Ni content <63 at.%Ni [9,13]. Although the EDS measurements do not indicate any differences in composition for the different grains in the sample, a 2 at.%Ni composition difference is within the experimental error of this analytical technique for grains with average size of (50 ± 10) nm as observed in the present type of samples. The lack of any 3R peaks in the XRD patterns indicates that this structure only occurs in very small amounts.

In order to determine if a martensitic transformation could occur in sample 35/100/24 (Table 1), a DSC measurement was performed. No exothermic or endothermic peaks were distinguished; however this can still be attributed to the low amount of this compact phase. Indeed, the Rietveld analysis of the sample indicated that the compact phase is present in sample 35/100/24 only with a concentration lower than 3%.

5. Conclusions

A stable intermetallic can be obtained for Ni–35 at.%Al and Ni–40 at.%Al by low energy mechanical milling. Evidence of more than one phase after 50 h of milling was detected by X-ray and TEM techniques, indicating a different phase stability when compared to high or intermediate energy ball milling. The time required to detect a higher percentage of intermetallics was shorter for the sample that contains more Al, which is related to the core–shell structure of the particles. A compact martensitic phase was found in the Ni–35 at.%Al sample after 100 h milling and a heat treatment at 600 °C for 24 h.

Acknowledgments

E. Zelaya and D. Schryvers thank the support of the MINCyT-FWO Project FW/09/03 VS.002.11N.

References

[1] D.B. Miracle, The physical and mechanical properties of NiAl, Acta Metall. Mat. 41 (3) (1993) 649–684.
[2] T.B. Massalski, Binary Alloy Phase Diagrams, ASM, 1986.
[3] S.A. Obregon, J.J. Andrade Gamboa, M.R. Esquivel, Synthesis of Al/containing $MmNi_5$ by mechanical alloying: Milling stages, structure parameters and thermal annealing, Int. J. Hydrogen Energy 37 (19) (2012) 14972–14977.
[4] C. Suryanarayana, Mechanical alloying and milling, C. Suryanarayana Prog. Mater. Sci. 46 (2001) 1–184.
[5] L. Lü, M.O. Lai, Mechanical Alloying, Kluwer Academic Publishers., 1998.
[6] K. Enami, S. Nenno, New ordered phase in tempered 63,8 Ni–Co–Al martensite, Trans. Jpn Inst. Met. 19 (1978) 571–580.
[7] K. Enami, S. Nenno, K Shimizu, Crystal structure internal twins of the Ni-36,8%Al martensite, Trans. Jpn Inst. Met. 14 (1973) 161.
[8] S. Chakravorty, C.M. Wayman, Thermoelastic martensitic transformation in beta prime Ni–Al alloys – 2. Electron microscopy, Metall. Trans. 7 (1976) 555–569.
[9] V.V. Martynov, K. Enami, L.G. Kbandros, A.V. Tkachenko, S. Nenno, Crystal structure of stress-induced thermal martensites in 63.1 at% Ni–Al alloy, Script Met 17 (1983) 1167–1171.
[10] F. Reynaud, Anomalies in the electron diffraction patterns of nickel-rich β′–NiAl alloys, Scripta Metall 11 (1977) 765–770.
[11] K. Enami, A. Nagasawa, S. Nenno, On the premartensitic transformation in the Ni–Al β1 alloy, Scripta Metall 12 (1978) 223–226.
[12] D. Schryvers, Microtwin sequences in thermoelastic Ni_xAl_{100-x} martensite studied by conventional and high-resolution transmission electron microscopy, Philos. Mag. 68 (1993) 1017–1032.
[13] J.H. Yang, C.M. Wayman, On the formation mechanism of Ni_5Al_3 in NiAl-base alloys: Part I. microstructures, lntermetallics 2 (1994) 111–119.
[14] D. Schryvers, Y. Ma, L. Toth, L.E. Tanner, Electron microscopy study of the formation of Ni_5Al_3 in a $Ni_{62.5}Al_{37.5}$ B2 alloy—I. Precipitation and growth, Acta Metall. Mater. 43 (11) (1995) 4045–4056.
[15] D. Schryvers, Y. Ma, A.L. Toth, L.E. Tanner, Electron microscopy study of the formation of Ni_5Al_3 in a $Ni_{62.5}Al_{37.5}$ B2 alloy—II. Plate crystallography, Acta Metall. Mater. 43 (11) (1995) 4057–4065.
[16] D. Schryvers, Y. Ma, In situ TEM study of the Ni_5Al_3 to B2 + $L1_2$ decomposition in $Ni_{65}Al_{35}$, Mater. Lett. 23 (1995) 105–111.
[17] P.L. Potapov, P. Ochin, J. Pons, D. Schryvers, Nanoscale inhomogeneities in melt-spun Ni–Al, Acta Mater. 48 (2000) 3833–3845.
[18] S.K. Pabi, B.S. Murty, Mechanism of mechanical alloying in Ni–Al and Cu–Zn systems, Mater. Sci. Eng. A214 (1996) 146–152.
[19] V.K. Portnoy, A.M. Blinov, I.A. Tomilin, V.N. Kuznetsov, T. Kulik, Formation of nickel aluminides by mechanical alloying and thermodynamics of interaction, J. Alloys Compd. 336 (2002) 196–201.
[20] L. Lu, M.O Lai, Mechanical alloying, vol. 4, Kluwer Academic Publisher, Boston, 1998.
[21] R.A. Young, A. Sakthivel, T.S. Moss, C.O. Paiva-Santos, DBWS-9411-an upgrade of the DBWS programs for Rietveld refinement with PC and mainframe computers, J. Appl. Crystallogr. 28 (1995) 366–367.
[22] T. Chen, J.M. Hampikian, N.N. Thadhani, Synthesis and characterization of mechanically alloyed and shock-consolidated nanocrystalline NiAl intermetallic, Acta Mater. 47 (8) (1999) 2567–2579.
[23] A. Guinier, D.L. Dexter, X-Ray Studies of Materials, Interscience Publishers, 1963.
[24] M. De Graef, Introduction to Conventional Transmission Electron Microscopy, Cambridge University Press, 2002.
[25] K. Otsuka, T. Ohba, M. Tokonami, C.M. Wayman, New description of long period stacking order structures of martensites in β-phase alloys, Scripta Metall. Mater 29 (1993) 1359–1364.